Giant resonances in ^{24}Mg and ^{28}Si from 240 MeV ^{6}Li scattering

X. Chen,[1] Y.-W. Lui,[2] H. L. Clark,[2] Y. Tokimoto,[2] and D. H. Youngblood[2]
[1]*Chemistry Department, Washington University, St. Louis, Missouri 63130, USA*
[2]*Cyclotron Institute, Texas A&M University, College Station, Texas 77843, USA*
(Received 31 March 2009; published 15 July 2009)

Elastic and inelastic scattering of 240 MeV ^{6}Li particles from ^{24}Mg and ^{28}Si were measured with the MDM spectrometer. Optical potential parameters for ^{6}Li + ^{24}Mg and ^{6}Li + ^{28}Si scattering systems were obtained by fitting elastic scattering with two different folding model potentials as well as W-S potentials. $E0$-$E3$ giant resonance strength distributions for ^{28}Si and ^{24}Mg were obtained. $E0$ strength corresponding to 106^{+34}_{-24}% of the EWSR was identified in ^{24}Mg and 80^{+35}_{-20}% was found for ^{28}Si between $E_x = 8.0$ to 40.0 MeV.

DOI: 10.1103/PhysRevC.80.014312 PACS number(s): 24.30.Cz, 25.70.Bc, 27.30.+t

I. INTRODUCTION

Measurements of the energies of the isoscalar giant monopole resonance (ISGMR) in many nuclei have provided the most effective constraints on the imcompressibility of nuclear matter K_{nm} [1]. A comparison of ISGMR energies with fully consistent HF-RPA calculations [2] yielded $K_{nm} =$ 230–240 MeV while a comparison with fully consistent relativistic random phase approximation (RRPA) [3,4] calculations resulted in $K_{nm} =$ 250–270 MeV. It was suggested [2,5–7] that the difference is mainly due to the differences in the symmetry energy coefficient J and its slope L associated with these models. Alpha inelastic scattering at small angles has been widely used to study the ISGMR in many stable medium and heavy nuclei, and studies of Sn and Cd isotopes have focused on the symmetry energy [8–11]. Extending these studies to unstable nuclei should improve the sensitivity to the symmetry energy. However for unstable nuclei [12], a helium target would have to be used for "α scattering," and they are not well suited for use in measurements of the GMR. Suitable ^{6}Li targets are straightforward, and giant resonances in ^{116}Sn have been studied with inelastic scattering of 240 MeV ^{6}Li ions [12]. The results obtained for the isoscalar monopole and quadrupole resonances in ^{116}Sn agreed well with previous studies using α particles, suggesting that 240 MeV ^{6}Li scattering is an alternate way to study the ISGMR in medium mass nuclei. In lighter nuclei, the strength of the GMR fragments and extends to higher excitation energy as shown in several α scattering experiments [13–16]. Separating these higher energy fragments from the continuum can be difficult. The relative continuum and GR contributions in α and ^{6}Li scattering might be quiet different, hence ^{6}Li scattering could provide complimentary information on giant resonances in light nuclei.

Isoscalar giant resonances in ^{24}Mg have been studied with 240 MeV α scattering [13] and 156 MeV ^{6}Li scattering [17]. The GMR strength distribution obtained with 240 MeV α scattering continues up to $E_x \sim 42$ MeV and 72 ± 10% of the $E0$ EWSR strength was identified. In Ref. [17] the authors report identifying ~100% of the $E0$ EWSR below $E_x =$ 23 MeV using 156 MeV ^{6}Li scattering, however Youngblood *et al.* [13] pointed out that an unconventional normalization of the data to the DWBA was used in Ref. [17], which could account for the discrepancy. Isoscalar giant resonances in ^{28}Si have been studied with α scattering in a series of works [16,18–20]. The $E0$ strength distributions obtained with 240 MeV α scattering extended up to $E_x \sim 42$ MeV and 81 ± 10% of the $E0$ EWSR strength was identified. A study of GR's in ^{24}Mg and ^{28}Si with 240 MeV ^{6}Li scattering might identify additional $E0$ strength not located in the α studies and provide more evidence of the suitability of ^{6}Li inverse scattering to study the GMR in unstable nuclei.

II. EXPERIMENTAL SETUP

The experimental technique has been described in Ref. [21] and is summarized briefly below. A beam of 240 MeV ^{6}Li particles from the Texas A&M University K500 superconducting cyclotron passed through a beam analysis system [22] and bombarded targets located in the target chamber of the multipole-dipole-multipole spectrometer (MDM) [23]. The targets were self-supporting foils, 7.56 mg/cm^2 thick natural Si and 4.35 mg/cm^2 thick Mg enriched to 99% in ^{24}Mg. The thicknesses of the targets were determined by measuring the energy loss of the 240 MeV ^{6}Li beam passing through the target. The horizontal acceptance of the spectrometer was 4° and ray tracing was used to reconstruct the scattering angle. The vertical acceptance was ±2°. The outgoing particles were detected by a 60 cm long focal plane detector. It contains four resistive wire proportional counters to measure position, as well as an ionization chamber to provide ΔE and a scintillator behind the ionization chamber to measure the energy deposited and provide a fast timing signal for each event. The principles of operation of the detector are similar to the detector described in Ref. [24] and the details of angle and position calibrations were described in Ref. [25]. Position resolution of approximately 0.9 mm and scattering angle resolution of about 0.09° were obtained. The out-of-plane scattering angle was not measured.

The spectrometer angles used for measuring elastic scattering and giant resonances of ^{24}Mg and ^{28}Si are listed in Table I. In the data analysis, data taken at each spectrometer angle was divided into ten angle bins, with each angle bin corresponding to $\Delta\theta \approx 0.4°$. The average angle for each angle bin was determined by integrating over the height of the slit and the width of the angle bin. The absolute differential cross

TABLE I. Spectrometer angles used for measuring elastic scattering and giant resonances. The numbers in parenthesis are the slit opening used (horizontal × vertical in degree).

	^{28}Si		^{24}Mg	
	Elastic	GR	Elastic	GR
	5°, 7°, 9°(4° × 2°)		5°, 7°, 9°(4° × 2°)	
θ_{spec}	11°, 13°, 15°, 17°, 19°, 21°, 23°, 26°, 29°, 32°, 35° (4° × 4°)	0°, 4° (4° × 4°)	11°, 13°, 15°, 17°, 19°, 21°, 23°, 26°, 29°, 32°, 35° (4° × 4°)	0°, 4°, 6° (4° × 4°)

section for each angle bin was obtained from the combination of yield, charge integration, target thickness, solid angle, and dead time correction. The cumulative uncertainties in target thickness, solid angle, etc., result in a ±10% uncertainty in absolute cross section.

III. ELASTIC SCATTERING AND INELASTIC SCATTERING TO LOW-LYING STATES OF ^{28}Si AND ^{24}Mg

The angular distributions of the cross sections for elastic scattering of ^{6}Li from ^{24}Mg and ^{28}Si are shown in Figs. 1 and 2, respectively. These data were fit using both W-S phenomenological potentials and folding potentials constructed by integrating nucleon-nucleon (NN) effective interactions over the interacting nuclei. The optical parameters which resulted in the best fit using W-S potentials are listed in Table II and the fits are shown in Figs. 1 and 2.

There are several NN effective interactions which have been used in folding calculations of elastic scattering, such as the JLM interaction [26], the S1Y interaction [27] and the M3Y interaction [28,29]. In this work we used both the M3Y-Paris NN effective interaction and JLM interactions. We previously used the M3Y interaction in the analysis of ^{116}Sn elastic scattering [21] and inelastic scattering to GR's [12]. A density dependent double folding calculation based on M3Y NN effective interaction was used in this work to obtain the real potential. Here the knock-on exchange contribution is estimated with a finite range approximation and the density dependence function introduced in Refs. [30–32] is used. A Woods-Saxon potential was used for the imaginary part of the optical potential.

Real and imaginary potentials were also calculated using the JLM NN effective interaction. The JLM interaction is a complex, energy and density dependent G-matrix interaction which is obtained from the Reid soft-core NN potential with the Brueckner-Hartree-Fock (BHF) approximation [26]. Starting from the potential for a nucleon of energy E traversing nuclear matter of density ρ

$$U_{NM}(\rho,E) = V(\rho,E) + iW(\rho,E), \tag{1}$$

where V and W are real and imaginary parts (for the expressions of V and W, see Ref. [33]), the density and energy dependent JLM NN effective interaction for heavy ion scattering can be obtained as

$$v(\rho,E) = \frac{V(\rho,E) + iW(\rho,E)}{\rho}. \tag{2}$$

The potential for heavy ion collisions thus is given by the folding integral

$$V(R) = \int \rho_T(r_T)\rho_P(r_P)v(\rho,E)\delta(\vec{s})\,d\vec{r}_T\,d\vec{r}_P, \tag{3}$$

where $\vec{s} = \vec{r}_T + \vec{R} - \vec{r}_P$, ρ_T is the density of the target and ρ_P is the density of the projectile. The local density is estimated as geometric average of the projectile and target density

$$\rho(\vec{s}) = \left[\rho_T\left(\vec{r}_T + \frac{\vec{s}}{2}\right)\rho_P\left(\vec{r}_P - \frac{\vec{s}}{2}\right)\right]^{1/2}. \tag{4}$$

When the folded potential obtained with the JLM interaction is used to analyze the elastic scattering data, the quality of the fit can be substantially improved by replacing the δ function in Eq. (3) by a finite range smearing function [26,34]

$$g(\vec{s}) = \left(\frac{1}{t\sqrt{\pi}}\right)^3 e^{-s^2/t^2}, \tag{5}$$

where t is the range parameter. With the smearing function included, the rms radii of the folded potential are increased, but the volume integrals do not change since the smearing functions are normalized to 1. There are substantial renormalization factors required for both real and imaginary parts of these folded potentials when they are used to analyze elastic scattering involving loosely bound nuclei, such as ^{6}Li and ^{7}Li

$$U(r) = N_V V_{\text{fold}}(r) + iN_W W_{\text{fold}}(r). \tag{6}$$

The strong couplings with breakup of the projectile and neutron transfer channel are responsible for these renormalizations [33].

Folding calculations with the density dependent M3Y NN interaction (called FCI in the following) are described in detail by Khoa [32], while folding calculations using the JLM effective interaction (called FCII in the following) are described by Carstoiu *et al.* [35], L. Trache *et al.* [33], and references therein. In FCI, a Fermi distribution (see Table III) was used for the target ground density and the cluster-orbital shell-model approximation [36] form was used for the ^{6}Li ground state density (see Eq. (8) of Ref. [21]). The real

TABLE II. Optical parameters obtained from fitting 240 MeV ^{6}Li elastic scattering from ^{28}Si and ^{24}Mg with W-S potentials.

Target	V (MeV)	r_0 (fm)	A (fm)	W (MeV)	r_{i0} (fm)	a_i (fm)	J_v (MeV fm^3)	J_w (MeV fm^3)	σ_r (mb)	χ^2
^{28}Si	143.34	0.720	0.937	32.13	1.004	0.921	261	125	1650	1.43
^{24}Mg	114.52	0.762	0.879	34.518	0.956	1.027	244	138	1680	1.14

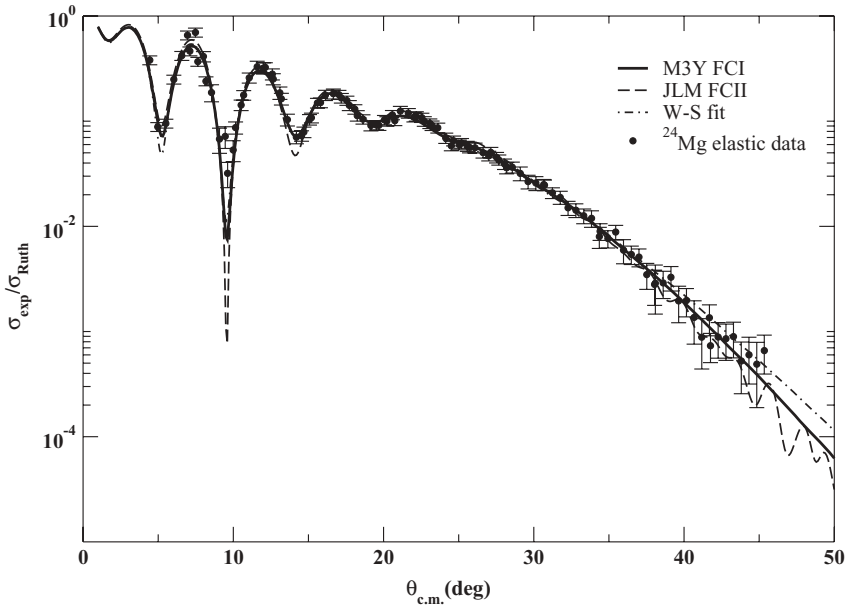

FIG. 1. Experimental angular distribution of the cross section (relative to the Rutherford cross section) and fits for ^{6}Li + ^{24}Mg elastic scattering using W-S potential (dash and dot curve), folding potential with CDM3Y6 NN interaction (black curve) and folding potential with JLM NN interaction (dash) are shown. The error bars indicate statistical and systematic errors.

part of optical potential is obtained by folding and a W-S phenomenological potential is used for the imaginary term. FCI was carried out with DFPD4 [37] and elastic scattering data were fitted with ECIS [38]. The optical parameters obtained are listed in Table IV. In FCII, HF densities [39,40] (see Table III) were used for both target and projectile. Both real and imaginary potentials were obtained from folding. The elastic scattering fit was carried out with OPTJLM1 [41]. The optical parameters obtained are shown in Table V. The angular distributions of the cross-sections calculated using both interactions are plotted along with the data in Fig. 1 for ^{24}Mg and Fig. 2 for ^{28}Si.

A scaling factor S_r on the radius of the real optical potential is necessary to fit the elastic scattering data for both ^{24}Mg and ^{28}Si when FCI is used. Folding calculations with different types of density dependent M3Y interactions such as CDM3Y4, CDM3Y5, CDM3Y6 (see Table I of Ref. [31]) give almost the same scaling factors for ^{24}Mg elastic scattering. Khoa [44] suggests that the need for such a scaling factor indicates that a repulsive surface correction of DPP is vital for a realistic description by the folding model. This is being explored as a separate topic. The fit to elastic scattering with the JLM folding calculation is not improved by a scaling factor on the radius. However there is an adjustable smearing factor **t** in the smearing function with the JLM interaction which greatly increases the ability of the folding form factor to simulate the radial dependence of DPP [35].

The volume integrals of the optical potentials were calculated for ^{6}Li scattering on ^{28}Si and ^{24}Mg. The spread of the volume integrals of the real potentials obtained for ^{28}Si with

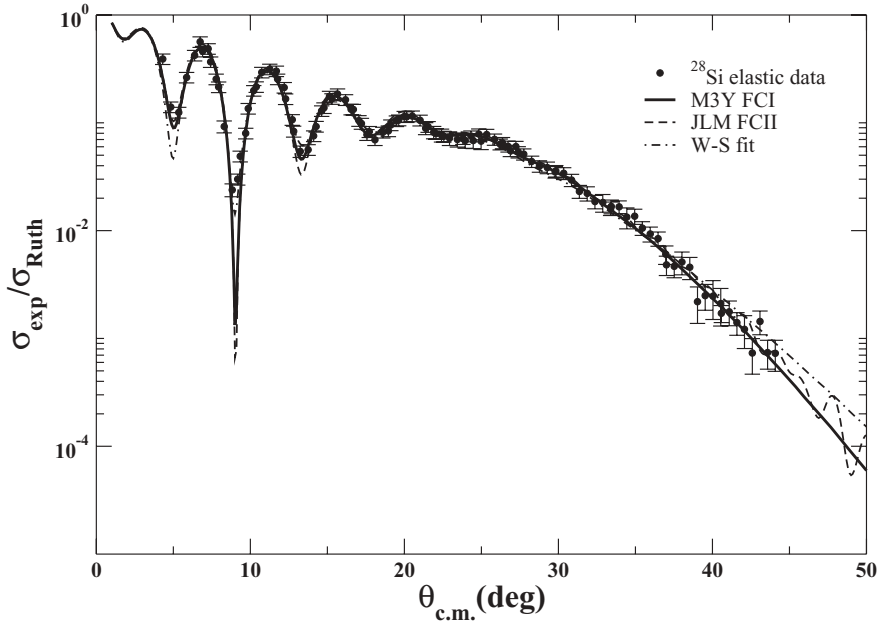

FIG. 2. Experimental angular distribution of the cross section (relative to the Rutherford cross section) and fits for ^{6}Li + ^{28}Si elastic scattering using W-S potential (dash and dot curve), folding potential with CDM3Y5 NN interaction (black curve) and folding potential with JLM NN interaction (dash) are shown. The error bars indicate statistical and systematic errors.

TABLE III. Density parameters used in the folding calculations. Den1 are Fermi distributions. HF stands for Hartree-Fock density. R_p, R_n, R_m are the root mean square radii of the calculated proton, neutron, and mass distributions, respectively.

Target	Density choice	ρ_0 (fm)	C (fm)	A (fm)	R_p (fm)	R_n (fm)	R_m (fm)
^{24}Mg	Den1 [42]	0.17	2.995	0.478	2.922	2.922	2.922
	HF [40]	–	–	–	2.928	2.906	2.917
^{28}Si	Den1 [43]	0.175	3.15	0.475	3.010	3.010	3.010
	HF [40]	–	–	–	3.059	3.031	3.045

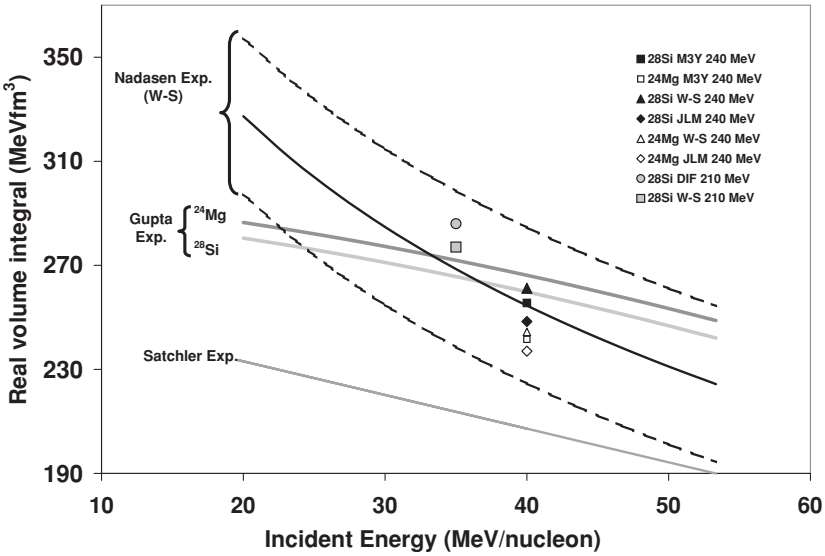

FIG. 3. The volume integral of the real part of the optical potential for ^{6}Li scattering on ^{28}Si and ^{24}Mg obtained with W-S model, folding model with JLM and M3Y effective NN interactions plotted versus incident beam energy. The black curve represents Nadasen *et al.*'s expression obtained with W-S potentials [45]. The area between the two dash lines represents the range of volume integral predicted by Nadasen *et al.* The gray and light gray curves represent Gupta and Murthy's expression for ^{24}Mg and ^{28}Si obtained with JLM nucleon-nucleus potentials [46]. The bottom gray curve represents Satchler's expression obtained with S1Y effective NN interaction [27]. Volume integrals obtained from Ref. [43] for 210 MeV ^{6}Li scattering on ^{28}Si are also plotted in the figure for comparison.

TABLE IV. Optical model parameters obtained from fits of elastic scattering with the folding calculations using the M3Y interaction. N_r is the renormalization factor for the real potential. S_r is the scaling factor for the real potential radius. W, r_{i0}, a_i are W-S parameters for the imaginary potentials. J_v and J_w are the volume integral per nucleon pair for the real and imaginary potentials, respectively. σ_r is the total reaction cross section.

Target	NN int.	Target density	N_r	S_r	W (MeV)	r_{i0} (fm)	a_i (fm)	J_v (MeV fm^3)	J_w (MeV fm^3)	σ_r (mb)	χ^2
^{24}Mg	CDM3Y5	Den1	0.823	1.062	58.67	0.731	1.204	242	154	1799	1.039
^{28}Si	CDM3Y5	Den1	0.887	1.0624	41.33	0.9049	1.048	256	136	1757	1.461

TABLE V. Optical potential parameters obtained from the fit of elastic scattering with folding calculations using the JLM interaction. N_r and N_w are the normalization factor for the real and imaginary potentials, respectively. t_r and t_w are range parameters for the real and imaginary potential, respectively.

Target	NN int.	Target density	N_r	t_r (fm)	N_w	t_w (fm)	J_v (MeV fm^3)	J_w (MeV fm^3)	σ_r (mb)	χ^2
^{24}Mg	JLM	HF	0.519	0.9559	0.862	2.586	237	144	1803	1.6
^{28}Si	JLM	HF	0.546	0.9165	0.825	2.4275	248	137	1734	1.94

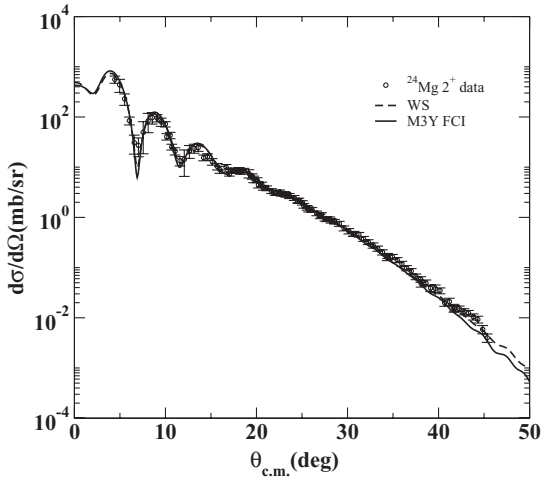

FIG. 4. The angular distributions of the differential cross sections for inelastic scattering to the 2^+ state of ^{24}Mg calculated with FCI and WS potentials along with the data points are plotted versus average center of mass angle.

the WS and two folding potentials is about 13 MeV · fm^3 while the spread for ^{24}Mg is 7 MeV · fm^3. The results are shown and compared with Nadasen *et al.*'s expression [45], Gupta and Murthy's expression [46], and Satchler's expression [27] in Fig. 3. Nadasen *et al.*'s expression is based on ^{6}Li-nucleus W-S potentials obtained from elastic scattering of 210 MeV ^{6}Li ions by ^{28}Si, ^{40}Ca, ^{90}Zr. It shows a logarithmic energy dependence of the form $J_R/6A = J_R^0/6A - \beta \ln E_{\rm lab}$ with $J_R^0/6A = 830 \pm 30$ MeV fm^3 and $\beta = 105 \pm 5$ MeV fm^3. Gupta and Murthy's expression is based on real volume integrals for the nucleon-nucleus optical potential derived from the microscopic calculation of Jeukenne *et al.* [26] by adding one additional term for the compositeness of the light projectile such as D, T, α, ^{3}He, and ^{6}Li. The volume integrals we obtain for ^{28}Si and ^{24}Mg are consistent with Nadasen *et al.*'s prediction and are close to Gupta and Murthy's prediction,

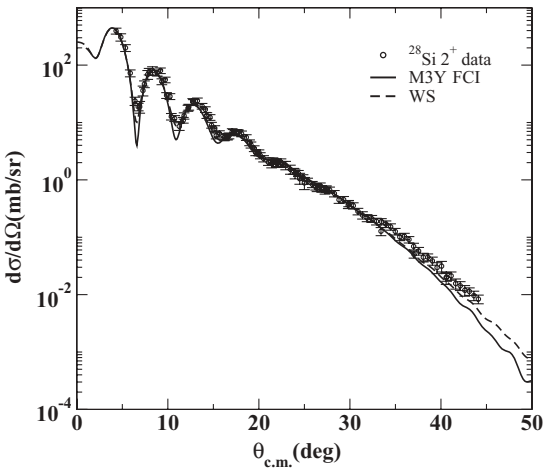

FIG. 5. The angular distributions of the differential cross sections for inelastic scattering to the low-lying 2^+ state of ^{28}Si calculated both with a W-S potential and with FCI along with the data points are plotted versus average center of mass angle.

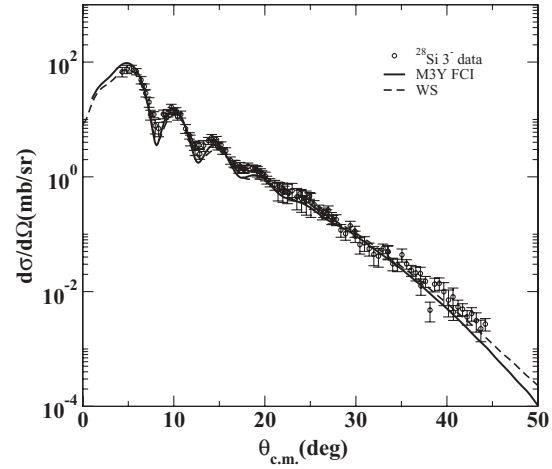

FIG. 6. The angular distributions of the differential cross sections for inelastic scattering to the low-lying 3^- state of ^{28}Si calculated both with a W-S potential model and with FCI along with the data points are plotted versus average center of mass angle.

but they are quite different from Satchler's prediction. (Note: Satchler's predictions are based on different target and projectile systems [27], and discrepancies as large as 50 MeV fm^3 were found between his predictions and previous folding model analyses of 210 MeV ^{6}Li scattering [43].)

As a test of the optical parameters obtained from elastic scattering, inelastic scattering data from excitations of well-known low-lying states in ^{24}Mg and ^{28}Si were compared to DWBA calculations with these parameters. As the χ^2 values for the elastic scattering fits with potentials obtained from the M3Y interaction and WS potentials were considerably better

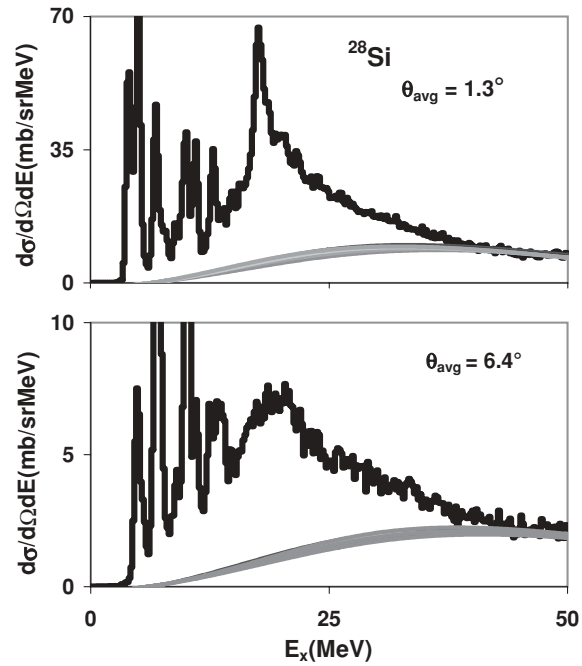

FIG. 7. Spectra obtained for ^{28}Si at average center of mass angles 1.3° and 6.4°. The gray curves are continuum shapes chosen for the analysis.

than with those obtained from the JLM interaction, DWBA calculations for ^{6}Li inelastic scattering to the low-lying 2^+ state of ^{24}Mg and to low-lying 2^+ and 3^- states of ^{28}Si were carried out with transition potentials obtained by the deformed potential model and FCI. In the deformed potential model calculations, both the real and imaginary parts of the transition potentials were obtained by taking first derivatives of W-S potentials [21]. In the folding model calculations such as FCI, the real parts of the transition potentials were calculated by folding the NN effective interaction over the densities and transition densities of the target and projectile [32], while the imaginary parts were constructed with the deformed potential model [47]. For the FCI calculations, the CDM3Y5 density dependent NN interaction was used and the Den1 form (as shown in Table III) was chosen as the target density for both ^{24}Mg and ^{28}Si. The transition potentials were calculated with DFPD4 and the cross sections were calculated with ECIS. The mass deformation parameters for the 2^+ and 3^- states were obtained from electromagnetic $B(EL)$ values by assuming that the mass and Coulomb deformation lengths are the same.

$B(EL)$ values for the 2^+ and 3^- states of ^{28}Si and the 2^+ state of ^{24}Mg were extracted by fitting the inelastic scattering cross section and are listed in Table VI. The $B(E2)$ values obtained for the ^{28}Si 2^+ state and ^{24}Mg 2^+ state obtained with the folding model calculations agree with the adopted value and with the value from electron scattering. The $B(E3)$ value obtained for the ^{28}Si 3^- state is about 1 standard deviation below the adopted value, but is consistent with the value obtained from electron scattering [48]. The $B(EL)$ values obtained with the deformed potential model are all smaller than the adopted value or the value from electron scattering. This is consistent with Beene *et al.*'s conclusions [49] that inelastic scattering analyzed with deformed potential calculations cannot reproduce electromagnetic transition probabilities. The calculated angular distribution for the 2^+ state in ^{24}Mg is plotted in Fig. 4 along with the data. The calculated angular

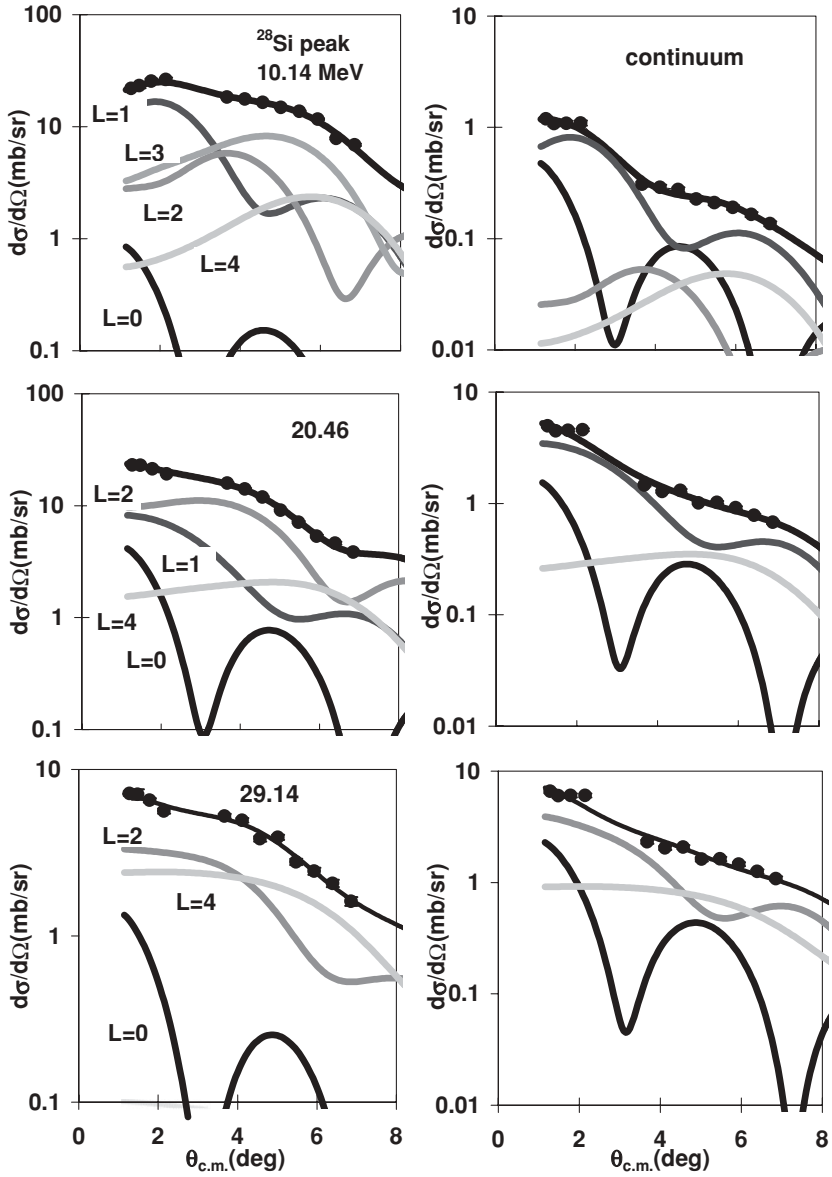

FIG. 8. Angular distributions of the cross section for ^{6}Li inelastic scattering from ^{28}Si for 0.8 MeV wide bins centered at E_x = 10.14, 20.46, 29.14 MeV along with DWBA fits. The left column shows those for the giant resonance peak while the right column shows those for the continuum.

TABLE VI. The $B(EL)$ values for 2^+ and 3^- states of ^{28}Si and the 2^+state of ^{24}Mg obtained with the deformed potential model and the double folding model. Adopted values of $B(E2)$ and $B(E3)$, as well as values extracted from electron scattering, are shown in the table. For $B(EL)$ values obtained from ^{6}Li scattering, the superscript errors represent statistical errors, while the subscript errors represent total errors including statistical and systematic errors.

Work	Model	^{28}Si $J^\pi = 2^+, E_x = 1.779$ MeV $B(E2)\,(e^2\,\mathrm{b}^2)$	^{28}Si $J^\pi = 3^-, E_x = 6.888$ MeV $B(E3)\,(e^2\,\mathrm{b}^3)$	^{24}Mg $J^\pi = 2^+, E_x = 1.369$ MeV $B(E2)\,(e^2\,\mathrm{b}^2)$
Present	DP	$0.0229^{\pm 0.0003}_{\pm 0.0023}$	$0.00135^{\pm 0.00002}_{\pm 0.00014}$	$0.0317^{\pm 0.0004}_{\pm 0.0032}$
	DDF	$0.0318^{\pm 0.0004}_{\pm 0.0032}$	$0.00311^{\pm 0.00005}_{\pm 0.00031}$	$0.0465^{\pm 0.0006}_{\pm 0.0047}$
Electron scattering	EM	0.0337 ± 0.0030 [50]	0.00387 ± 0.00075 [48]	0.0420 ± 0.0025 [51]
	Adopted value	0.0326 ± 0.0012 [52]	0.0042 ± 0.0005 [53]	0.0432 ± 0.0011 [52]

distributions for 2^+ and 3^-states of ^{28}Si are plotted in Figs. 5 and 6, respectively, along with data.

IV. GIANT RESONANCE STUDY

A. Data analysis

Inelastic scattering of ^{6}Li from both ^{28}Si and ^{24}Mg excited into the giant resonance region was measured with the spectrometer at 0° and 4° and 6° for ^{24}Mg only. The excitation energy spectrum between 8 MeV and 40 MeV for each angle (see Sec. II) was divided into a peak and a continuum and was sliced into energy bins each with a width about 0.8 MeV and the angular distributions for each energy bin were obtained. The origins of and method of choosing the continuum have been discussed in previous papers [25,54]. The strength distributions for $E0$-$E3$ transitions were obtained from these angular distributions with a multipole decomposition technique [13,55,56] where the experimental distributions are fit by a sum of angular distributions calculated for $L = 0, 1, 2, 3, 4$ transitions. The transition potentials for $E0$ through $E4$ transitions were calculated using the M3Y-Paris NN effective interaction by folding as described above for the low-lying states. The transition densities used for $L \geqslant 2$ transition potentials were obtained using the Bohr-Mottelson (B-M) collective model [57] while those used for ISGMR were obtained with the scaling model [57,58] and those for the ISGDR were obtained following the collective formalism given by Harakeh and Dieperink [59], recognizing that their formalism is for one magnetic substate only [16]. The angular distributions of the differential cross sections for $E0$-$E4$ transitions in each energy bin were obtained with DWBA calculations using the potentials obtained with the M3Y-Paris NN effective interaction (FCI folding—Table IV). The uncertainties in strengths were estimated by adding (in quadrature) the uncertainty from the multipole fits to the standard deviations of all the fits obtained with different continuum choices. The uncertainties of the centroid energy and rms width were obtained as described in Ref. [12].

Excitation energy spectra for ^{28}Si obtained at average center of mass angles 1.3°, and 6.4° are shown in Fig. 7 with gray curves representing the continuum choices. The folding optical potentials were obtained with the CDM3Y5 NN interaction and with density choice Den1 (as shown in Table III). Angular distributions of differential cross sections for the giant resonance peak and background are shown in Fig. 8 along with DWBA fits for three energy bins with average excitation energies 10.14 MeV, 20.46 MeV, and 29.14 MeV. Sample excitation energy spectra for ^{24}Mg with average center of mass angles 1.3°, 4.7°, and 9.5° are shown in Fig. 9 with gray curves representing the continuum choices.

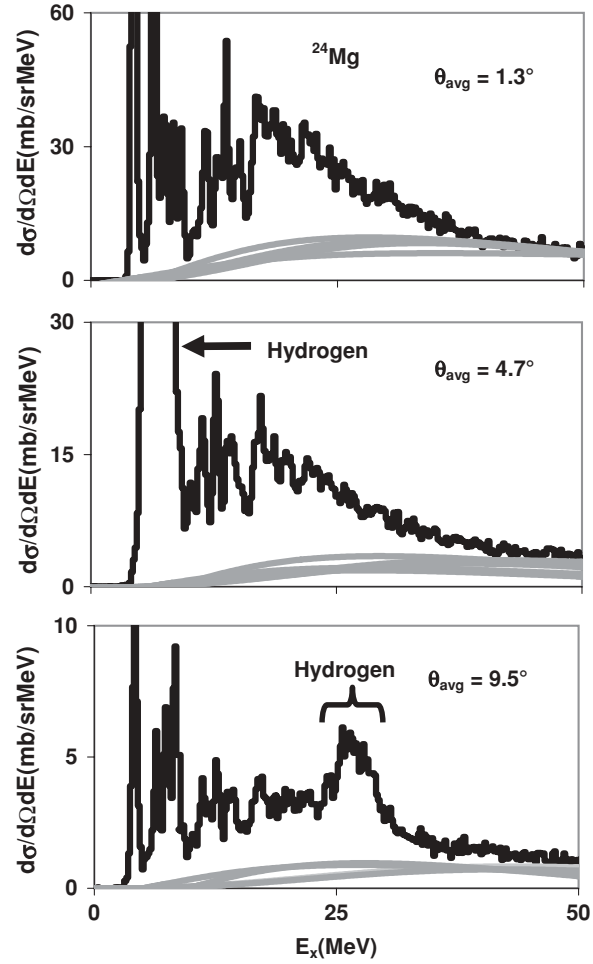

FIG. 9. Spectra obtained for ^{24}Mg at average center of mass angles 1.3°, 4.7°, and 9.5°. The gray curves are different continuum choices for the analysis. The broad structures pointed by the arrow or covered by the bracket are caused by ^{6}Li scattering from hydrogen in the target.

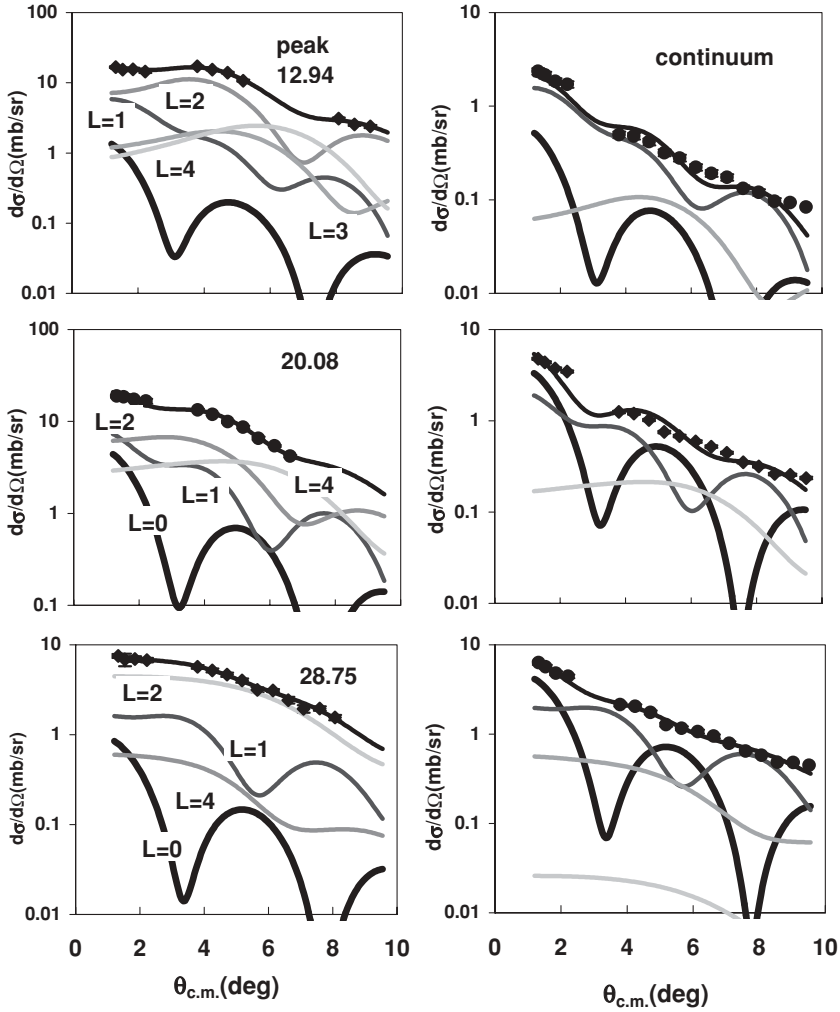

FIG. 10. Angular distributions of the cross section for inelastic scattering from ^{24}Mg for 0.8 MeV wide bins centered at $E_x =$ 12.94, 20.08, 28.75 MeV along with DWBA fits. The left column shows those for the giant resonance peak while the right column shows those for the continuum.

Angular distributions of differential cross sections for the giant resonance peak and background are shown in Fig. 10 along with DWBA fits for three energy bins with average excitation energies 12.94 MeV, 20.08 MeV, and 28.75 MeV.

B. ^{28}Si

The $E0$, $E1$, $E2$, and $E3$ strength distributions obtained for ^{28}Si are shown in Fig. 11 along with those obtained from α scattering. The multipole parameters obtained for ^{28}Si are summarized and compared with those from α scattering in Table VII. The centroid, $(m1/m0)$, rms width, and percentage of the EWSR are calculated for the excitation range measured (8 to 40 MeV), as well as the ranges 8 to 22.4 MeV and 22.4 to 40 MeV.

The $E0$ strength distribution extracted in this work agrees well with that obtained from α scattering [16] (see Fig. 11). The strength extracted corresponds to 80^{+35}_{-20}% of the $E0$ EWSR with a centroid of $20.59^{+0.78}_{-0.33}$ MeV and an rms width $5.78^{+1.34}_{-0.34}$ MeV, in good agreement with that observed in α scattering which corresponds to 81 ± 10% of the $E0$ EWSR with a centroid of 21.25 ± 0.38 MeV and an rms width 6.4 ± 0.6 MeV.

The $E2$ strength distribution extracted for 8 MeV $< E_x <$ 22.4 MeV in this work agrees well with α scattering as can be seen in the figure. Above 22 MeV, however, the $E2$ strength extracted from ^{6}Li scattering is higher than that obtained from α scattering, 64 ± 6% of the $E2$ EWSR compared to 18 ± 2% given in Ref. [16].

Much more ISGDR strength was identified in this work than in the α scattering [12]. A total of 84^{+21}_{-11}% of the $E1$ EWSR was identified with ^{6}Li scattering whereas only 15 ± 4% was identified in α scattering and there is a peak around 26.0 MeV which does not show up in α scattering.

There is little agreement between the $E3$ strength distributions obtained with ^{6}Li and α scattering. In this work strength corresponding to only about 30% of the $E3$ EWSR was identified, most above 22 MeV, whereas 10% of the $E3$ EWSR was identified in α scattering, most of which was below $E_x = 22$ MeV [16].

In the most recent paper on ^{28}Si, Youngblood *et al.* [19] reported a new analysis of α inelastic scattering data with the assumption that all of the cross sections are due to multipole processes in the excitation range $E_x < 42$ MeV. No continuum was subtracted. This analysis showed that $E0$ strength extracted is only weakly dependent on the assumption made about the continuum. The $E0$ strength

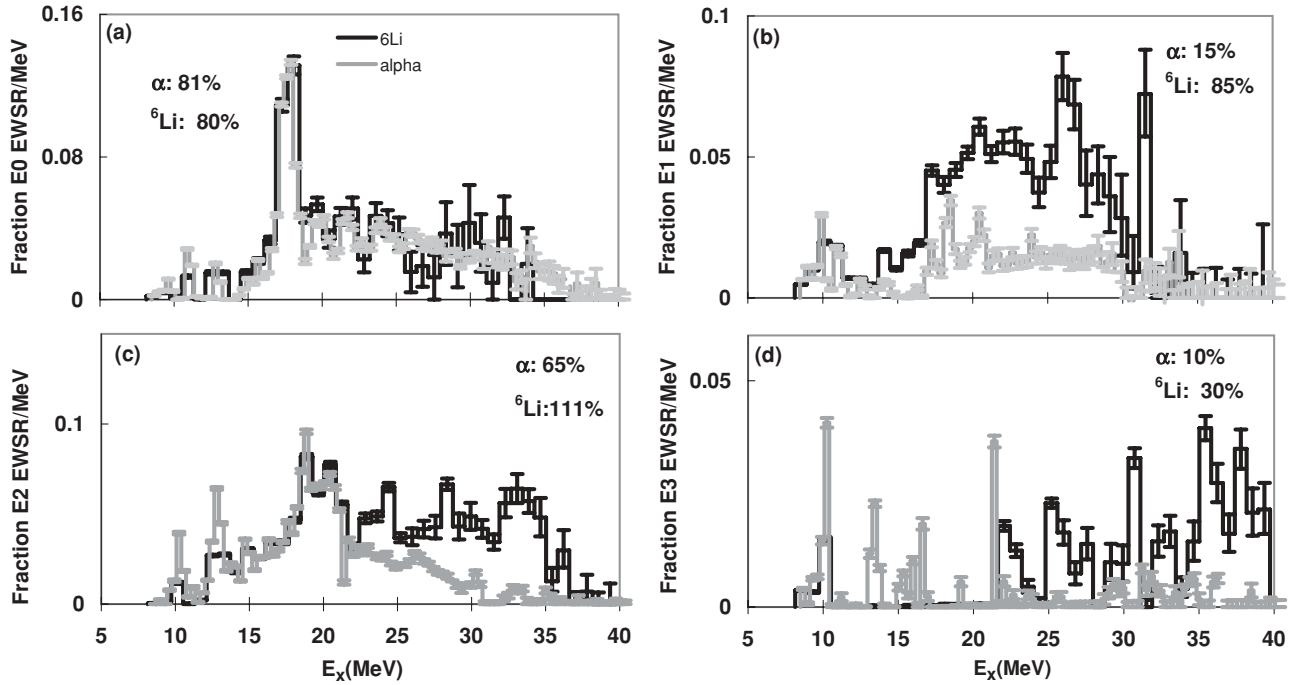

FIG. 11. The black curves show $E0$, $E1$, $E2$, and $E3$ strength distributions for ^{28}Si [(a): $E0$, (b): $E1$, (c): $E2$, and (d): $E3$] obtained from analysis of ^{6}Li inelastic scattering. The gray curves show those obtained with α inelastic scattering [16]. Error bars represent the uncertainty due to the fitting of the angular distributions and different choices of the continuum.

obtained, $74 \pm 7\%$ of the $E0$ EWSR, the centroid energy (m_1/m_0) 20.89 ± 0.38 MeV, and rms width 5.9 ± 0.6 MeV all agree within the errors with those from Ref. [16] and from this work (see Fig. 12) where continuum subtractions were made. For other multipolarities, the continuum choice had a strong effect on the strength extracted. The largest effect was on the $E1$ strength, which continues to rise with excitation energy, and far exceeded the sum rule when no continuum was subtracted. Below $E_x \sim 23$ MeV the $E1$ distributions obtained from α scattering (no continuum) and ^{6}Li scattering are in fair agreement, but diverge sharply at higher excitation (see Fig. 13). The authors of Ref. [19] point out that the "$E1$"

TABLE VII. Multipole parameters obtained for ^{28}Si in this work compared to those obtained from analysis of α scattering.

	This work				α scattering [16]			
	E_x range (MeV)	m_1/m_0 (MeV)	rms width (MeV)	EWSR (%)	E_x range (MeV)	m_1/m_0 (MeV)	rms width (MeV)	EWSR (%)
$E0$	8.0–22.4	17.60 ± 0.17	2.67 ± 0.17	48 ± 6	8.0–22.5	17.27 ± 0.38	3.04 ± 0.6	42 ± 4
	22.4–40.0	$27.72^{+0.73}_{-0.25}$	$3.21^{+1.34}_{-0.34}$	31^{+30}_{-13}	22.5–40.0	28.22 ± 0.38	3.75 ± 0.6	39 ± 4
	8.0–40.0	$20.59^{+0.78}_{-0.33}$	$5.78^{+1.34}_{-0.34}$	80^{+35}_{-20}	8.0–40.0	$21.25^{+0.38}_{-0.38}$	6.4 ± 0.6	81 ± 10
$E1$	8.0–22.4	16.9 ± 0.17	$3.77^{+0.74}_{-0.19}$	40 ± 4	8.0–22.5	15.3 ± 0.60	4.75 ± 0.7	8 ± 0.8
	22.4–40.0	$27.27^{+0.34}_{-0.20}$	$2.69^{+0.74}_{-0.19}$	38^{+19}_{-10}	22.5–40.0	27.56 ± 0.60	3.05 ± 0.7	7 ± 0.7
	8.0–40.0	$21.17^{-0.41}_{-0.24}$	$5.87^{+0.74}_{-0.19}$	84^{+21}_{-11}	8.0–40.0	19.27 ± 0.60	6.9 ± 0.7	15 ± 4
$E2$	8.0–22.4	17.25 ± 0.17	3.02 ± 0.23	47 ± 5	8.0–22.5	16.59 ± 0.25	3.5 ± 0.6	47 ± 5
	22.4–40.0	$29.22^{+0.20}_{-0.19}$	3.81 ± 0.23	64 ± 6	22.5–40.0	27.21 ± 0.25	2.98 ± 0.6	18 ± 2
	8.0–40.0	$22.69^{+0.23}_{-0.20}$	6.94 ± 0.23	111 ± 16	8.0–40.0	18.53 ± 0.25	4.7 ± 0.6	65 ± 9
$E3$	8.0–22.4	$12.94^{+0.25}_{-0.19}$	6.54 ± 0.18	4^{+5}_{-1}	8.0–22.5	13.31 ± 0.25	4.57 ± 0.6	7 ± 0.7
	22.4–40.0	32.15 ± 0.17	4.48 ± 0.18	27 ± 3	22.5–40.0	33.32 ± 0.25	3.48 ± 0.6	3 ± 0.3
	8.0–40.0	27.71 ± 0.24	8.09 ± 0.18	31^{+7}_{-6}	8.0–40.0	16.3 ± 0.25	9.22 ± 0.6	10 ± 1

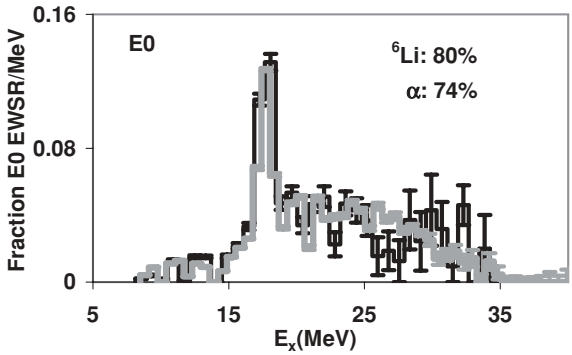

FIG. 12. $E0$ strength distribution obtained from analysis of ^{6}Li scattering compared to that obtained from analysis of α scattering (gray curve) without continuum subtraction [19].

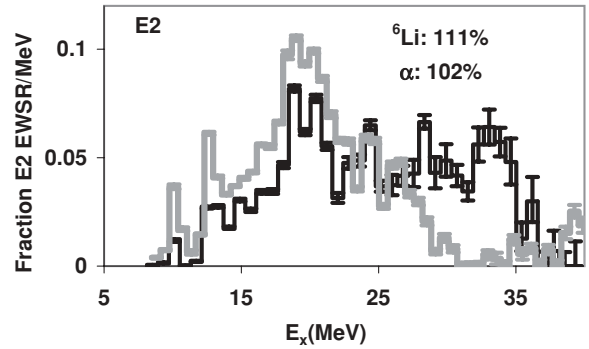

FIG. 14. $E2$ strength distribution obtained from analysis of ^{6}Li scattering compared to that obtained from analysis of α scattering (gray curve) without continuum subtraction [19].

strength extracted in α scattering is extremely sensitive to the choice of a continuum, and that the total "$E1$" strength far exceeds the sum rule, suggesting that there are other processes (not multipole excitation) in α scattering that have an angular distribution mimicking that of an $E1$ excitation. The disagreement in $E1$ strength obtained with ^{6}Li and α projectiles suggests that these "continuum" processes (whatever they are) are different with the two projectiles. The percentage of $E2$ EWSR reported in that paper agrees with $111 \pm 16\%$ extracted in ^{6}Li scattering, but the distribution of the strength is somewhat different (see Fig. 14).

C. ^{24}Mg

The $E0$, $E1$, $E2$, and $E3$ strength distributions obtained for ^{24}Mg are compared in Figs. 15 and 16 to those obtained from two different analyses of α scattering. Giant resonance parameters obtained for ^{24}Mg are summarized and compared with those from α scattering and 156 MeV ^{6}Li scattering in Table VIII.

Up to $E_x \sim 15$ MeV, the $E0$ strength obtained with α's and with ^{6}Li agree well, but for 15 MeV $< E_x <$ 32 MeV considerably more strength is seen with the ^{6}Li than with α particles. Above $E_x \sim 32$ MeV little net strength is seen in the ^{6}Li analysis, though the errors are significant, whereas

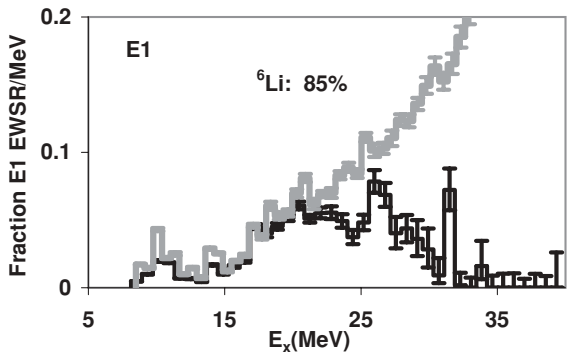

FIG. 13. $E1$ strength distribution obtained from analysis of ^{6}Li scattering compared to that obtained from analysis of α scattering (gray curve) without continuum subtraction [19].

both α analyses report significant $E0$ strength above 32 MeV. The total ^{24}Mg strength extracted in the energy range 8.6 to 38.6 MeV in this work ($106^{+34}_{-24}\%$ of the $E0$ EWSR), is larger by a little more than 1 standard deviation than the $72 \pm 10\%$ reported by Ref. [13] obtained in α scattering but within errors is in agreement with $82 \pm 9\%$ obtained in a new analysis of the α scattering [60]. Dennert *et al.* [17] reported $97 \pm 15\%$ of the $E0$ EWSR in the much narrower region $E_x = 10.0$–23.1 MeV using 156 MeV ^{6}Li scattering. However, Youngblood *et al.* [13] pointed out that Dennert *et al.* used a nonconventional normalization of the DWBA to the angular distribution (see Fig. 3 in Ref. [17]), in which the peak of the experimental angular distribution is about a factor of 2 below the peak of the DWBA calculation. This resulted in the reported $E0$ strength being about a factor of 2 higher. If Dennert *et al.*'s result is divided by this factor of 2, the adjusted $E0$ strength in the range $E_x = 10.0$–20.2 MeV corresponds to 34% of the $E0$ EWSR with a centroid energy 16.66 ± 0.5 MeV and rms width 2.48 ± 0.5 MeV, which is in excellent agreement with the strength obtained in this work between 10.2–20.6 MeV, $35 \pm 5\%$ of the $E0$ EWSR with a centroid energy 16.88 ± 0.17 MeV and rms width 2.13 ± 0.17 MeV (see Fig. 17 and Table VIII).

The $E2$ strength extracted for ^{24}Mg in this work corresponding to $76^{+14}_{-12}\%$ of the $E2$ EWSR with a centroid energy of $20.23^{+0.25}_{-0.20}$ MeV and an rms width of $6.29^{+0.34}_{-0.25}$ MeV, is in agreement with that obtained with the new analysis of the α data [60] which corresponds to $89 \pm 9\%$ of the $E2$ EWSR with a centroid of 19.92 ± 0.18 MeV and an rms width of $7.25^{+0.25}_{-0.20}$ MeV. The percentage of the $E2$ EWSR obtained also agrees with $72 \pm 10\%$ of the $E2$ EWSR given in Ref. [13], however, the strength given in Ref. [13] has a lower centroid energy of 16.9 ± 0.6 MeV and a much smaller rms width of 3.4 ± 0.6 MeV. As can be seen in Fig. 15, the $E2$ strength from ^{6}Li scattering and α scattering agree well except in the region from $E_x = 25$–28 MeV, where strong components show up at different energies.

The isoscalar $E1$ strength obtained in this experiment corresponds to $84^{+24}_{-21}\%$ of the $E1$ EWSR, which is much higher than $27^{+26}_{-14}\%$ reported in Ref. [13] (note: the original value $81^{+26}_{-14}\%$ in Table IV of Ref. [13] should be divided by 3 due to the transition density correction for ISGDR). In the new analysis of α scattering data, the $E1$ strength obtained

TABLE VIII. Multipole parameters obtained for ^{24}Mg in this work compared to those obtained from analysis of α scattering and from 156 MeV ^{6}Li scattering.

L	^{6}Li scattering					α scattering				
	Ref.	E_x energy (MeV)	m_1/m_0 (MeV)	rms width (MeV)	EWSR (%)	Ref.	E_x range (MeV)	m_1/m_0 (MeV)	rms width (MeV)	EWSR (%)
0	This work	10.2–20.6	$16.88^{+0.17}_{-0.17}$	2.13 ± 0.17	35 ± 5	[13]	10.1–20.9	16.31 ± 0.6[a]	2.62 ± 0.74	27 ± 4
		8.6–38.6	$21.35^{+0.37}_{-0.26}$	$4.98^{+0.68}_{-0.32}$	106^{+34}_{-24}		9.0–41.0	21.0 ± 0.6	7.3 ± 1.2	72 ± 10
	156 MeV ^{6}Li [17]	10.0–20.2	16.66 ± 0.5[a]	2.48 ± 0.5[a]	68 ± 12	[60]	10.2–20.4	$16.44^{+0.33}_{-0.25}$	$2.48^{+0.48}_{-0.23}$	24 ± 4
		10.0–23.1	18.3 ± 0.5	4.8 ± 0.5	97 ± 15		9.0–41.0	$21.93^{+0.33}_{-0.25}$	$6.53^{+0.47}_{-0.23}$	82 ± 9
1	This work	10.2–20.6	$14.75^{+0.20}_{-0.17}$	2.29 ± 0.17	10 ± 3	[13]	10.1–20.9	14.68 ± 2.21	3.14 ± 0.97	12^{+11}_{-5}
							9.0–41.0	18.8 ± 1.7	6.7 ± 1.0	27^{+26}_{-11}
		8.6–38.6	$26.56^{+0.29}_{-0.26}$	$6.42^{+0.29}_{-0.27}$	84^{+24}_{-21}	[60]	10.2–20.4	$16.12^{+0.23}_{-0.20}$	$3.33^{+0.68}_{-0.49}$	16 ± 5
							9.0–41.0	$22.70^{+0.23}_{-0.20}$	$6.19^{+0.67}_{-0.49}$	65 ± 8
2	This work	10.2–20.6	15.79 ± 0.17	2.58 ± 0.17	30 ± 4	[13]	10.1–20.9	15.07 ± 0.6[a]	2.07 ± 0.6[a]	51^{+5}_{-8}
							9.0–41.0	16.9 ± 0.6	3.4 ± 0.6	72 ± 10
		8.6–38.6	$20.23^{+0.25}_{-0.20}$	$6.29^{+0.34}_{-0.25}$	76^{+14}_{-12}	[60]	10.2–20.4	15.56 ± 0.18	$2.93^{+0.25}_{-0.20}$	36 ± 4
							9.0–41.0	$19.92^{+0.18}_{-0.18}$	$7.25^{+0.25}_{-0.20}$	89 ± 9
3	This work	8.6–38.6	$18.54^{+1.40}_{-0.38}$	$5.85^{+0.28}_{-0.19}$	3^{+4}_{-1}	[13]	9.0–41.0	25.2 ± 1.0	4.5 ± 1.2	31^{+9}_{-6}
						[60]	9.0–41.0	$25.43^{+0.37}_{-0.23}$	$8.31^{+0.23}_{-0.22}$	42 ± 5

[a]Assume the uncertainty is the same as in the total energy range.

overlaps nicely with that obtained in this experiment below 27 MeV as can be seen in Fig. 15, but the strong peaks seen from ~27 to 36 MeV in the ^{6}Li data are not seen in the α data.

Little $E3$ strength was located in ^{24}Mg in this experiment, with only about 3% of the $E3$ EWSR identified, compared to α scattering where 31% of the $E3$ EWSR was reported in Ref. [13] and 42% of the $E3$ EWSR was identified in the new analysis of α scattering.

D. Comparison of ^{6}Li and α scattering for giant resonance studies

Cross sections calculated for the peak of the angular distributions for ^{6}Li and α scattering exciting ^{28}Si are shown for $L = 0$–3 transitions at four excitation energies from 15–40 MeV in Table IX. The peak differential cross sections for $E0$ excitation with ^{6}Li scattering and with α scattering at $E_x = 15$ MeV are about the same, but the $E0$ cross section decreases faster at higher excitation with ^{6}Li scattering than it does with α scattering. At $E_x = 40$ MeV, the peak $E0$ cross section for transitions excited with ^{6}Li scattering is ~2 mb/sr, but is ~11 mb/sr with α scattering. At all energies the ratio of the $E0$ cross section to those of each of the other multipoles is considerably less in ^{6}Li scattering than in α scattering. In Fig. 18, spectra obtained for ^{28}Si with ^{6}Li and α scattering are compared and the differential cross section for ^{6}Li scattering goes below that for α scattering around 40 MeV, suggesting that the processes that make up the continuum are lower in ^{6}Li scattering. This apparent lower continuum at least partially offsets the lower $E0$ cross sections at higher excitation. However, the very low peak cross section for $E0$ transitions above 40 MeV makes it difficult to extract reliable $E0$ strength above $E_x = 40$ MeV with ^{6}Li scattering.

TABLE IX. The maximum differential cross section obtained with DWBA calculations for ^{28}Si with $L = 0$–3 excitation in α and ^{6}Li inelastic scattering.

E_x(MeV)	Max. dσ/dΩ in ^{6}Li inelastic scattering (mb/sr)				Max. dσ/dΩ in α inelastic scattering (mb/sr)			
	$L = 0$	$L = 1$	$L = 2$	$L = 3$	$L = 0$	$L = 1$	$L = 2$	$L = 3$
15	361	460	331	428	343	170	228	206
30	21.4	32.1	66.6	143	53.7	29.4	69.0	82.3
35	7.25	13.0	35.4	89.5	25.8	16.5	47.3	61.4
40	2.29	5.54	17.8	49.9	11.3	8.9	32.2	49.0

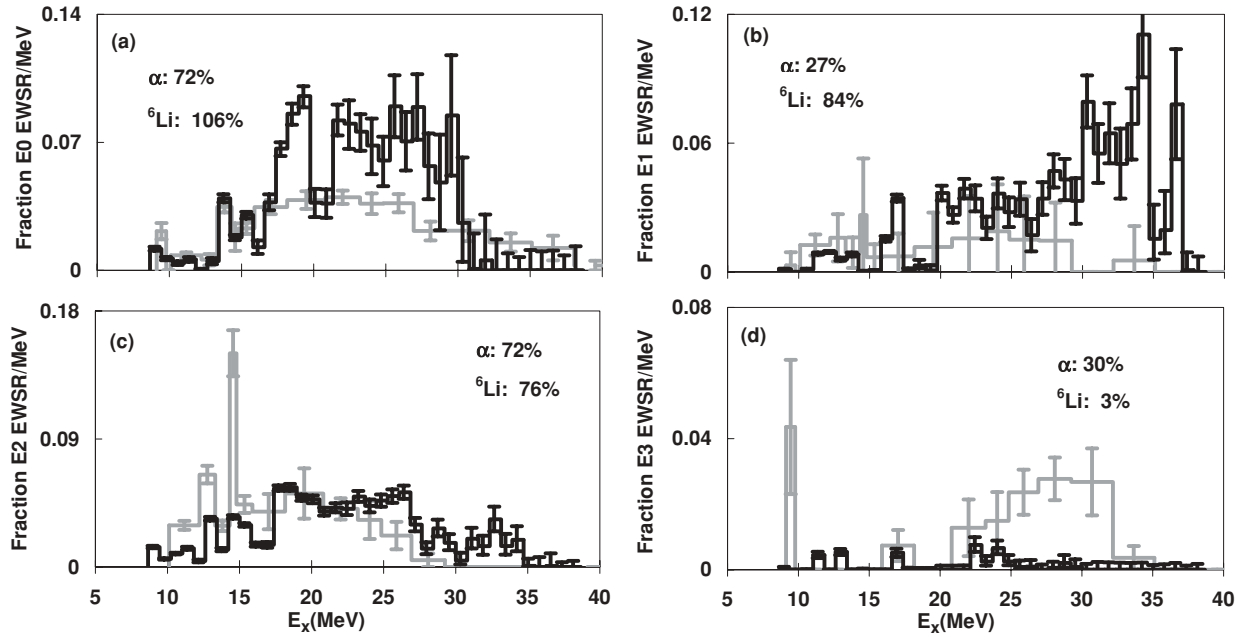

FIG. 15. The black curves show multipole EWSR strength distributions for ^{24}Mg [(a): $E0$, (b): $E1$, (c): $E2$, and (d): $E3$] obtained from analysis of ^{6}Li inelastic scattering. The gray curves show $E0$, $E1$, $E2$, and $E3$ strength distributions [13] obtained with α inelastic scattering. Error bars represent the uncertainty due to the fitting of the angular distributions and different choices of the continuum.

E. Comparison to QRPA calculations

Péru *et al.* [61] used the quasiparticle random phase approximation (QRPA) based on Hartree-Fock-Bogoliubov states (HFB) obtained with the Gogny D1S effective force [62,63], to calculate the ISGMR, ISGDR and ISGQR strength distributions for ^{24}Mg and ^{28}Si. The results are shown in Fig. 19 for ^{28}Si and Fig. 20 for ^{24}Mg and along with the strength distributions obtained in this work and from α scattering.

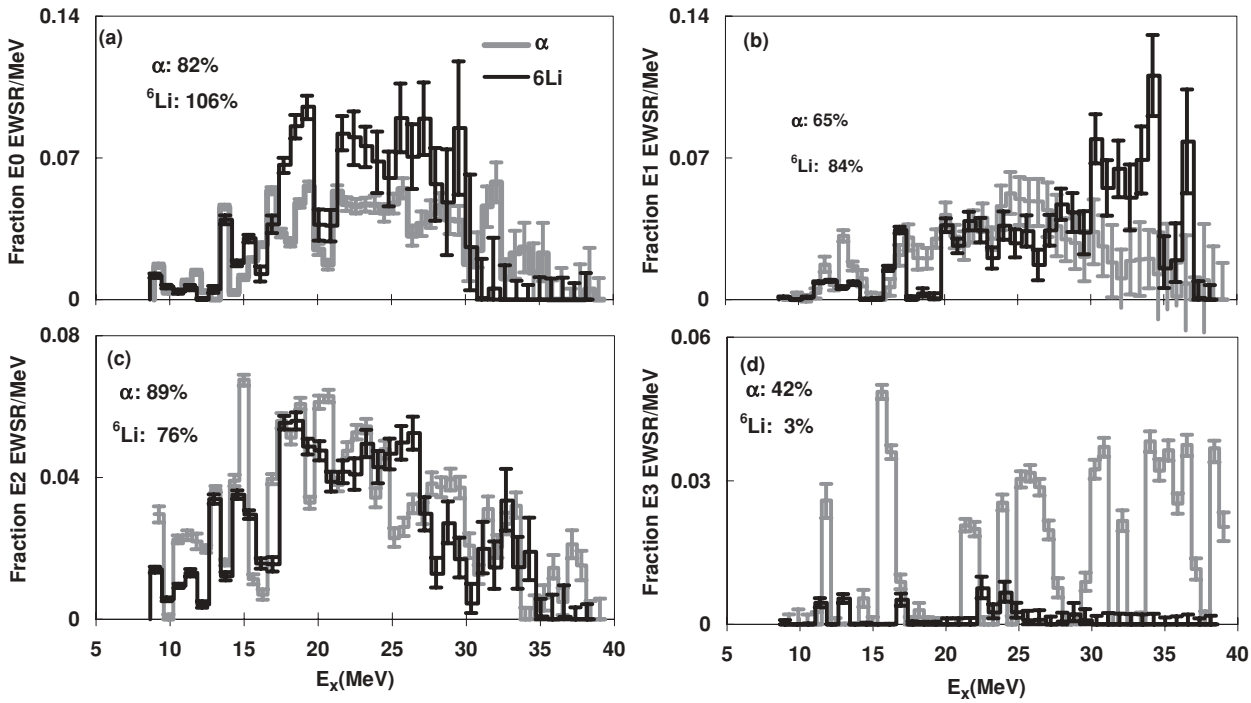

FIG. 16. The black curves show multipole EWSR strength distributions for ^{24}Mg [(a): $E0$, (b): $E1$, (c): $E2$, and (d): $E3$] obtained from analysis of ^{6}Li inelastic scattering. The gray curves show those obtained with new analysis of α inelastic scattering [60]. Error bars represent the uncertainty due to the fitting of the angular distributions and different choices of the continuum.

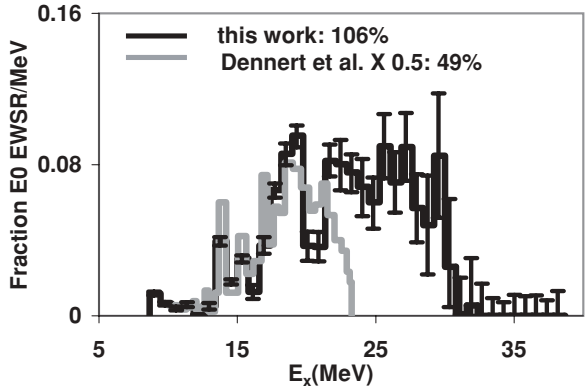

FIG. 17. $E0$ strength distribution obtained for ^{24}Mg (black line) in this work compared to that obtained from previous 156 MeV ^{6}Li scattering [17] multiplied by 0.5 (gray line). See the text for discussion of the 0.5 factor. The percentages shown in the figure represent the total EWSR strength found.

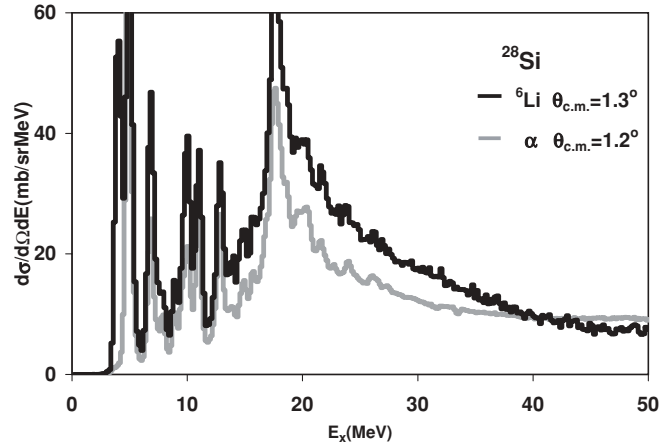

FIG. 18. The excitation energy spectra obtained in ^{6}Li scattering (black curve) at $\theta_{\text{c.m.}} = 1.3^{\circ}$ and in α scattering (gray curve) at $\theta_{\text{c.m.}} = 1.2^{\circ}$.

The $E0$ EWSR strength for ^{28}Si from the calculation has a peak around 20 MeV which is about 2 MeV higher than the peak seen in the experiment, otherwise they are in reasonable agreement. The $E0$ strength distribution calculated for ^{24}Mg is in reasonable agreement with the distribution obtained from the ^{6}Li scattering, but here the peaks from the calculation lie at lower energy than those observed in the experiment For ^{28}Si, the $E1$ strength distribution from calculations actually agree well with ^{6}Li scattering at high excitation, but the peak around ∼21 MeV is absent in the data, while the $E2$ strength from ^{6}Li scattering is spread more broadly than the calculation indicates. For ^{24}Mg, $E1$ strength distribution from

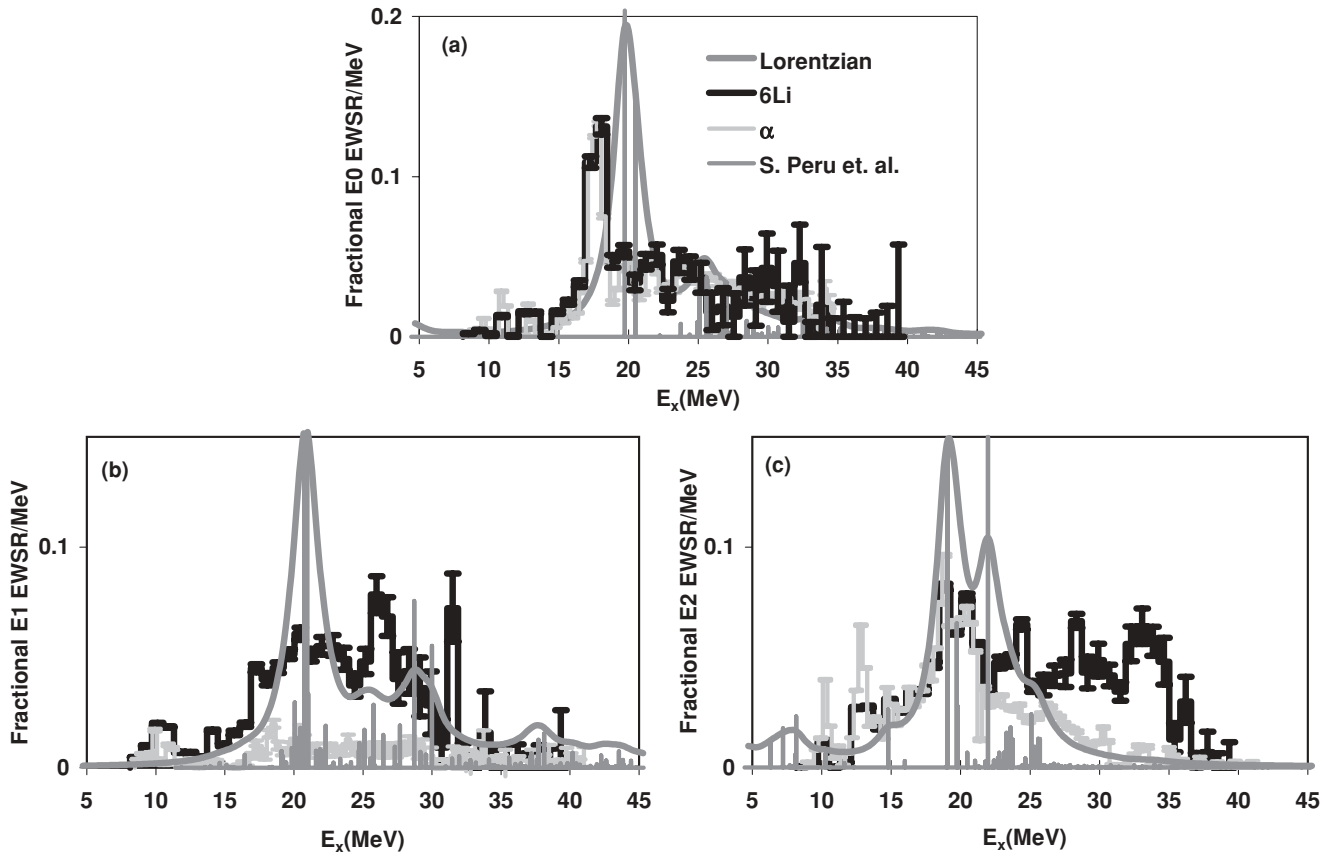

FIG. 19. $E0$–$E2$ strength distributions [(a): $E0$, (b): $E1$, and (c): $E2$] of ^{28}Si calculated by Péru *et al.* [61] with QRPA + HBF theory (shown as straight gray discrete lines), compared to that obtained in this work (black line) and in α scattering (light gray lines). The gray smooth curves represent the convolutions of calculated discrete spectra with 2 MeV width Lorentzian distributions.

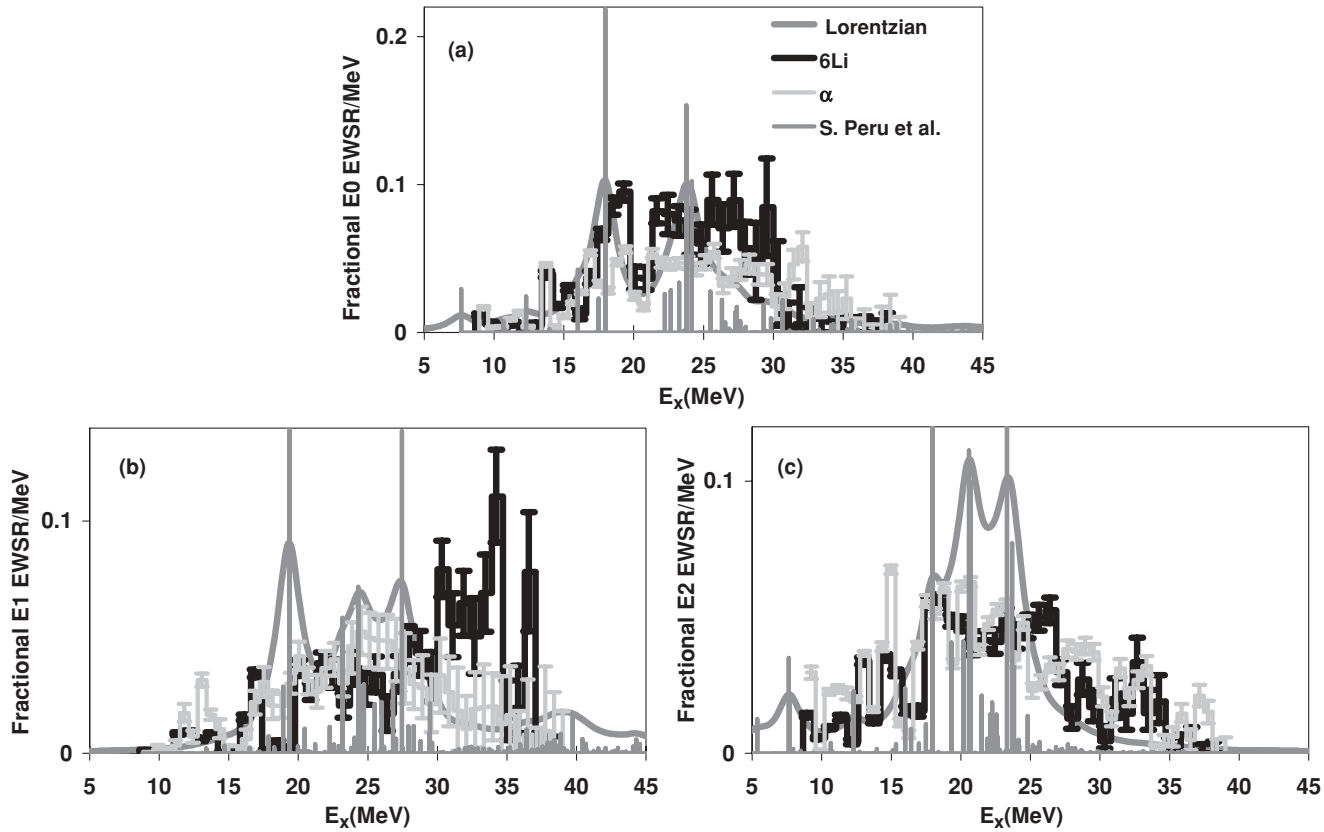

FIG. 20. $E0$–$E2$ strength distributions of ^{24}Mg [(a): $E0$, (b): $E1$, and (c): $E2$] calculated by Péru *et al.* [61] with QRPA + HBF theory (shown as straight discrete gray line), compared to those obtained in this work (black line) and in α scattering (light gray line). The smooth gray curves represent the convolutions of calculated discrete spectra with 2 MeV width Lorentzian distributions.

the calculations is quite different from that seen with ^{6}Li scattering but agrees well with α scattering at higher excitation. For the $E2$ strength distribution of ^{24}Mg, both calculations and ^{6}Li scattering show two peaks between 15–30 MeV, but the peaks are broader and the interval is wider in the experiment.

V. SUMMARY

Elastic and inelastic scattering of 240 MeV ^{6}Li particles from ^{24}Mg and ^{28}Si were measured with the MDM spectrometer. Optical parameters were obtained and tested by extracting $B(EL)$ values for low lying states. The optical potential parameters for ^{6}Li + ^{24}Mg and ^{6}Li + ^{28}Si scattering systems were obtained by fitting elastic scattering with two different folding model potentials as well as W-S potentials. The optical potential parameters obtained with the folding model from an M3Y NN potential were used to analyze giant resonance data with multipole decomposition techniques. The $E0$-$E3$ giant resonance strength distributions for ^{28}Si and ^{24}Mg were obtained and compared to those from 240 MeV α scattering and 156 MeV ^{6}Li scattering.

The $E0$ strength distribution obtained for ^{28}Si agrees very well with that from α scattering, but more $E0$ strength is seen in ^{24}Mg than with α scattering, except for $E_x >$ 32 MeV. There are some significant differences in the $E1$ and $E2$ strength distributions obtained for both ^{28}Si and ^{24}Mg and those obtained with α scattering, however the $E1$ distributions obtained from α scattering have been shown [19] to be very sensitive to assumptions about the continuum. Little $E3$ strength was identified in the ^{6}Li experiments, and there was little correlation with what was seen in α scattering. Except for the $E3$ strength, these results are consistent with the ^{116}Sn study [12] where the $E0$ distributions obtained with ^{6}Li and α scattering were in good agreement, while there were some differences in $E2$ strength distributions, and considerably more $E1$ strength was seen with the ^{6}Li scattering. The $E3$ strength seen in ^{116}Sn with α scattering is in agreement with that expected ($2\hbar\omega$ strength ∼75% of EWSR) [54], whereas considerably more was seen with ^{6}Li scattering.

The reasonable agreement of the $E0$ strength in ^{24}Mg, ^{28}Si, and ^{116}Sn obtained with α and ^{6}Li scattering suggests that 40 MeV/nucleon inelastic scattering using ^{6}Li as a projectile or a target is a viable way to study the ISGMR with the lower continuum somewhat offsetting the lower $E0$ cross sections in ^{6}Li scattering at higher excitation. The differences for the other multipoles could be due to several factors. The ^{6}Li data taken for these experiments had significantly less statistical accuracy that the α data, which could be particularly important for broad strength distributions sitting on a continuum. In addition, the continuum in 240 MeV α scattering has an angular distribution consistent with mostly $E1$ strength (but would considerably exceed the $E1$ EWSR, suggesting that other processes are responsible for much of this strength), making the separation of the broad $E1$ distribution from the continuum difficult.

The continuum in ^{6}Li scattering might be expected to be of different origin than in α scattering due in part to the low binding energy of ^{6}Li, and particularly at higher excitation, it is fit by a sum of several multipoles including $L = 0$, 1, 2, and 3. This and the fact that the continuum is weaker in ^{6}Li scattering considerably reduces the effects of continuum choice on $E1$ strength extracted from ^{6}Li scattering. However the presence of stronger components in the continuum with angular distributions similar to those of $L = 0, 2, 3$ transitions makes strength distributions extracted for those multipoles more sensitive to the continuum.

ACKNOWLEDGMENTS

We thank Dr. D. T. Khoa and Mr. Hoang Sy Than for their help and providing the computer codes to do the CDM3Yn folding calculations and cross section calculations. We thank Dr. Florin Carstoiu and Dr. Livius Trache for their help and providing computer code in JLM folding calculations. We also thank Dr. S. Péru *et al.* for providing their calculation results. This work was supported in part by the US Department of Energy under Grant No. DE-FG02-93ER40773 and by the Robert A. Welch Foundation under Grant A-0558.

[1] D. H. Youngblood, H. L. Clark, and Y.-W. Lui, Phys. Rev. Lett. **82**, 691 (1999).
[2] S. Shlomo, V. Kolomietz, and G. Colò, Eur. Phys. J. A **30**, 23 (2006).
[3] Z.-y. Ma, N. Van Giai, A. Wandelt *et al.*, Nucl. Phys. **A686**, 173 (2001).
[4] D. Vretenar, T. Nikšić, and P. Ring, Phys. Rev. C **68**, 024310 (2003).
[5] J. Piekarewicz, Phys. Rev. C **66**, 034305 (2002).
[6] S. Shlomo, B. K. Agrawal, and A. V. Kim, Nucl. Phys. **A734**, 589 (2004).
[7] B. K. Agrawal, S. Shlomo, and V. Kim Au, Phys. Rev. C **68**, 031304(R) (2003).
[8] Y.-W. Lui, D. H. Youngblood, H. L. Clark *et al.*, Acta Phys. Pol. B **36**, 1107 (2005).
[9] U. Garg, T. Li, S. Okumura *et al.*, Nucl. Phys. **A788**, 36 (2007).
[10] Y.-W. Lui, D. H. Youngblood, Y. Tokimoto *et al.*, Phys. Rev. C **70**, 014307 (2004).
[11] Y.-W. Lui, D. H. Youngblood, Y. Tokimoto, H. L. Clark, and B. John, Phys. Rev. C **69**, 034611 (2004).
[12] X. Chen, Y.-W. Lui, H. L. Clark *et al.*, Phys. Rev. C **79**, 024320 (2009).
[13] D. H. Youngblood, Y.-W. Lui, and H. L. Clark, Phys. Rev. C **60**, 014304 (1999).
[14] Y.-W. Lui, H. L. Clark, and D. H. Youngblood, Phys. Rev. C **64**, 064308 (2001).
[15] B. John, Y. Tokimoto, Y. W. Lui, H. L. Clark, X. Chen, and D. H. Youngblood, Phys. Rev. C **68**, 014305 (2003).
[16] D. H. Youngblood, Y.-W. Lui, and H. L. Clark, Phys. Rev. C **65**, 034302 (2002).
[17] H. Dennert, E. Aschenauer, and W. Eyrich *et al.*, Phys. Rev. C **52**, 3195 (1995).
[18] D. H. Youngblood, H. L. Clark, and Y.-W. Lui, Phys. Rev. C **57**, 1134 (1998).
[19] D. H. Youngblood, Y.-W. Lui, and H. L. Clark, Phys. Rev. C **76**, 027304 (2007).
[20] Y.-W. Lui, J. D. Bronson, D. H. Youngblood, Y. Toba, and U. Garg, Phys. Rev. C **31**, 1643 (1985).
[21] X. Chen, Y.-W. Lui, H. L. Clark *et al.*, Phys. Rev. C **76**, 054606 (2007).
[22] D. H. Youngblood and J. D. Bronson, Nucl. Instrum. Methods Phys. Res. A **361**, 37 (1995).
[23] D. M. Pringle, W. N. Catford, J. S. Winfield *et al.*, Nucl. Instrum. Methods Phys. Res. A **245**, 230 (1986).
[24] D. H. Youngblood, Y.-W. Lui, H. L. Clark *et al.*, Nucl. Instrum. Methods Phys. Res. A **361**, 539 (1995).
[25] D. H. Youngblood, Y.-W. Lui, and H. L. Clark, Phys. Rev. C **55**, 2811 (1997).
[26] J. P. Jeukenne, A. Lejeune, and C. Mahaux, Phys. Rev. C **16**, 80 (1977).
[27] G. R. Satchler, Nucl. Phys. **A579**, 241 (1994).
[28] G. Bertsch, J. Borysowicz, H. McManus *et al.*, Nucl. Phys. **A284**, 399 (1977).
[29] N. Anantaraman, H. Toki, and G. F. Bertsch, Nucl. Phys. **A398**, 269 (1983).
[30] D. T. Khoa and W. von Oertzen, Phys. Lett. **B304**, 8 (1993).
[31] D. T. Khoa, G. R. Satchler, and W. von Oertzen, Phys. Rev. C **56**, 954 (1997).
[32] D. T. Khoa and G. R. Satchler, Nucl. Phys. **A668**, 3 (2000).
[33] L. Trache, A. Azhari, H. L. Clark *et al.*, Phys. Rev. C **61**, 024612 (2000).
[34] E. Bauge, J. P. Delaroche, and M. Girod, Phys. Rev. C **58**, 1118 (1998).
[35] F. Carstoiu, L. Trache, R. E. Tribble *et al.*, Phys. Rev. C **70**, 054610 (2004).
[36] A. A. Korsheninnikov, E. Y. Nikolskii, C. A. Bertulani *et al.*, Nucl. Phys. **A617**, 45 (1997).
[37] D. T. Khoa (unpublished, 2000).
[38] J. Raynal (unpublished).
[39] M. Beiner and R. J. Lombard, Ann. Phys. (NY) **86**, 262 (1974).
[40] F. Carstoiu and R. J. Lombard, Ann. Phys. (NY) **217**, 279 (1992).
[41] F. Carstoiu (unpublished).
[42] M. Pignanelli, S. Micheletti, R. De Leo, S. Brandenburg, and M. N. Harakeh, Phys. Rev. C **33**, 40 (1986).
[43] M. El-Azab Farid and M. A. Hassanain, Nucl. Phys. **A678**, 39 (2000).
[44] D. T. Khoa (private communication, 2008).
[45] A. Nadasen, M. McMaster, M. Fingal *et al.*, Phys. Rev. C **39**, 536 (1989).
[46] S. K. Gupta and K. H. N. Murthy, Z. Phys. A **307**, 187 (1982).
[47] G. R. Satchler and D. T. Khoa, Phys. Rev. C **55**, 285 (1997).
[48] S. Yen, R. J. Sobie, T. E. Drake, H. Zarek, C. F. Williamson, S. Kowalski, and C. P. Sargent, Phys. Rev. C **27**, 1939 (1983).
[49] J. R. Beene, D. J. Horen, and G. R. Satchler, Phys. Rev. C **48**, 3128 (1993).
[50] S. W. Brain, A. Johnston, W. A. Gillespie *et al.*, J. Phys. G **3**, 821 (1977).
[51] A. Johnston and T. E. Drake, J. Phys. A **7**, 898 (1974).
[52] S. Raman, C. W. Nestor, and P. Tikkanen, At. Data Nucl. Data Tables **78**, 1 (2001).

[53] T. Kibedi and R. H. Spear, At. Data Nucl. Data Tables **80**, 35 (2002).
[54] D. H. Youngblood, Y.-W. Lui, H. L. Clark *et al.*, Phys. Rev. C **69**, 034315 (2004).
[55] D. H. Youngblood, Nucl. Phys. **A687**, 1c (2001).
[56] D. H. Youngblood, Y.-W. Lui, and H. L. Clark, Phys. Rev. C **63**, 067301 (2001).
[57] G. R. Satchler, *Direct Nuclear Reactions* (Oxford University Press, New York, 1983).
[58] H. Uberall, *Electron Scattering from Complex Nuclei* (Academic Press, New York, 1971).
[59] M. N. Harakeh and A. E. L. Dieperink, Phys. Rev. C **23**, 2329 (1981).
[60] D. H. Youngblood (private communication, 2007).
[61] S. Peru, H. Goutte, and J. F. Berger, Nucl. Phys. **A788**, 44 (2007).
[62] J. Dechargé and D. Gogny, Phys. Rev. C **21**, 1568 (1980).
[63] J. F. Berger, M. Girod, and D. Gogny, Comput. Phys. Commun. **63**, 365 (1991).